Progressive Collapse Resistance of Emulative Precast Concrete Frames with Various Reinforcing Details

Kai Qian[1] M. ASCE, Shi-Lin Liang[2], Feng Fu[3] CEng, F. ASCE, and Yi Li[4]

ABSTRACT

In this paper, three precast concrete (PC) frames and one cast-in-situ reinforced concrete (RC) frame were cast and tested to investigate the load resisting mechanisms of emulative PC frames with various reinforcing details to resist progressive collapse. In the beams of PC frames, the top reinforcement was continuous without curtailment while the bottom reinforcement had different anchorage strength. Test results indicated that, in the event of middle column removal, similar to RC frame, beam action, compressive arch action (CAA), and tensile catenary action (TCA) could be developed sequentially in PC frames with emulative connections, PC frames with sufficient anchorage length or additional bottom U-shaped bar passing through the middle joint could obtain similar level of CAA capacity as RC frame. However, they may achieve relatively lower TCA capacity due to higher bond strength between the top reinforcement and cast-in-situ topping layer in beams, owing to higher concrete strength in the topping layer, resulting in earlier fracture of the beam top reinforcements. Conversely, PC frames with insufficient anchorage could achieve comparable TCA capacity as RC frame. However, their CAA capacity was less than that of RC frames due to pulling-out failure of bottom reinforcements, preventing further development of strain hardening at beam action and CAA stages. Based on test results and analytical studies, it was found that, similar to RC frame, PC frames with emulative connections could provide sufficient rotational capacity to ensure development of tie-force as required by the design guidelines.

Keywords: Progressive Collapse; Precast Concrete; Emulative Connection; Experimental Tests

---

[1]Professor, College of Civil Engineering and Architecture at Guilin University of Technology, Guilin, China, 541004, College of Civil Engineering and Architecture at Guangxi University, Nanning, China

530004 (corresponding author), qiankai@gxu.edu.cn
[2]Research Student, College of Civil Engineering and Architecture at Guangxi University, Nanning, China 530004, liangshilin@st.gxu.edu.cn
[3]Senior Lecturer [4](Associate Professor) in Structural Engineering, School of Mathematics, Computer Science and Engineering, City, University of London, U.K., Feng.Fu.1@city.ac.uk
[4]Associate Professor, Key Laboratory of Urban Security and Disaster Engineering of Ministry of Education, Beijing University of Technology, Beijing 1000124, China, yili@bjut.edu.au

INTRODUCTION

Progressive collapse is defined as the spread of an initial local failure from element to element, which eventually results in the collapse of an entire structure or a disproportionately large part of it (ASCE SEI7 2010). The collapse of Alfred P. Murrah Federal Building, Oklahoma City, 1995 and twin towers in World Trade Center, New York, 2001 have all demonstrated the disastrous consequences of progressive collapse. To minimize the potential of such disaster, alternate load path (ALP) method, which is one of direct design methods from DoD (2010) and GSA (2013), is commonly utilized for practical design and analysis due to its threat-independent feature. In ALP method, various column removal scenarios are analyzed to assess the load redistribution capacity of the remaining building to bridge the initial damage (Stevens et al 2011; Fu,2016).

Based on ALP method, extensive tests (Sasani 2008; Sasani and Kropelnicki 2008; Yi et al. 2008; Sadek et al. 2011; Qian et al.2020; Qian and Li 2012a, b; Yu et al. 2013; Lew et al. 2014; Qian et al. 2015; Valipour et al. 2015; Shan et al. 2016; Lu et al. 2017; Lin et al. 2019; Yu et al. 2020; Deng et al. 2020) had been carried out. Sasani (2008) and Sasani and Kropelnicki (2008) carried out pioneer in-situ tests to quantify the dynamic behavior of RC frames subjected to column removal explosively. However, as the column longitudinal reinforcement was not clearly removed in the tests, the measured dynamic response in these in-situ tests was not obvious and only elastic response was captured. In addition, these in-situ dynamic tests indicated that upper stories worked together to redistribute the load, caused by the removed columns. Therefore, several dynamic tests (Qian and Li 2012b; Yu et al. 2014; Qian and Li 2017) relied on single-story

beam-column sub-assemblages were carried out to study the behavior of prototype multi-story frames equivalently. These dynamic tests indicated that the internal force may be amplified due to dynamic effects (Qian and Li 2012b). However, the dynamic effects will not change the failure mode and mobilization of load resisting mechanisms (Qian et al. 2020). Therefore, majority of existing tests regarding progressive collapse were single-story beam-column sub-assemblages subjected to quasi-static loading regime (Orton et al. 2008; Su et al. 2009; Qian and Li 2013; Yu et al. 2013; Qian et al. 2016; Ren et al. 2016; Yu et al. 2020; Deng et al. 2020). Although extensive tests were carried out to investigate the load resisting mechanism of RC frames subjected to different column missing scenarios, tests on precast concrete (PC) frames against progressive collapse were rare. Kang and Tan (2015; 2017) investigated performance of PC beam-column sub-assemblages with emulative connections subjected to column removal scenarios. Qian and Li (2018; 2019) experimentally quantified the load resisting mechanism of PC beam-column sub-structures with dry connections to resist progressive collapse. The effects of PC slabs were incorporated in Qian and Li (2018). It should be noted that the load resisting mechanisms of PC frames against progressive collapse varies in different types of beam-column connections. Thus, more studies are needed for deeper understanding of the progressive collapse resistance of PC frames with different beam-column connections or reinforcing details. For this reason, in this paper, three emulative PC beam-column sub-assemblages with different reinforcement details in beam-column connections were tested to quantify the effects of connection details on load resisting mechanisms of emulative PC frames. One additional RC beam-column sub-assemblages were also tested just as a reference test.

EXPERIMENTAL PROGRAM

Frame Design

The prototype building used in the tests was a nine-story moment resisting frame, which was non-seismically designed in accordance with ACI 318-14 (2014) and PCI handbook (PCI 2010). The design live load (LL) and dead load (DL) were 2.0 kPa and 5.5 kPa, respectively. Similar to the tests of Yu and Tan (2013), in this study, a series of beam-column sub-assemblages, composed of two beams, two enlarged side columns, and one middle column stub, were extracted from the prototype building for test. They were one-half scaled due to spacing and capacity limitation of the lab. Three PC frames (IA, SA, and UB) and one RC frame (RC) were designed and tested. As shown in Table 1, the notation "IA" denoted PC frame with Insufficient Anchorage for beam bottom reinforcements in the connection. "SA" represented PC frame with Sufficient Anchorage for beam bottom reinforcements in the connection. "UB" indicated PC frame with additional U-shaped bars passing through the middle joint, while the beam bottom reinforcements were bent up 90° and terminated at the beam end. In the fabrication of PC frames, the process can be divided into following steps. Firstly, the precast units (hatched area in Fig. 1) were casted. Then, the horizontal interfaces were grinded 4 mm deep intentionally to enhance the bond between precast elements and cast-in-situ toppings. After assembling PC columns and beams, additional U-shaped bars were added passing through the joints continually for UB. Finally, 50 mm depth topping layer and remaining part of the joints were casted on site.

For RC, as shown in Fig. 1(a), the bottom reinforcements in beam were continuous with curtailment. Moreover, the curtailment of longitudinal of bottom rebar followed the prototype frame design. The beam cross section was 250 mm×150 mm with shear link of R6@100 throughout the whole span. As shown in Fig. 1(b), the beam bottom reinforcements of IA were

straight lap-spliced with an anchorage length of 230 mm, which was less than the required length of 365 mm in accordance with ACI 318-14 (2014) and thus, the anchorage strength for the bottom reinforcements was insufficient. This frame was designed to study the influence of insufficient anchorage strength on the progressive collapse behavior of PC frames. For comparison, as shown in Fig. 1(c), the bottom reinforcements of SA were bent up 90° and protruded into joint to achieve sufficient anchorage strength. As shown in Fig. 1(d), UB has U-shaped trough with length of 370 mm in each beam end, its bottom reinforcements in PC beams were bent up 90° and terminated at beam ends. To continuously connect the PC components, two U-shaped bottom bars were added passing through the middle joints.

Material Properties

The material properties of reinforcement are tabulated in Table 2. Based on cylinder tests, the concrete compressive strength of RC frame on test day was 32 MPa. For PC frames, the first batch concrete used for precast units had a compressive strength of 36 MPa while the second batch concrete for cast-in-situ topping was 47 MPa, as required by PCI (2010).

Test Setup and Instrumentation

Fig. 2 illustrates the test setup and instrumentation layout. The side column was pin supported and connected to an A-frame by two rollers installed horizontally. To release redundant horizontal constraint from the pin support, a series of steel rollers [Item 8 in Fig. 2(b)] were placed beneath the pin support. The middle column was removed notionally before test to simulate the initial damage. Displacement-controlled loading method was applied on top of the missing column location through a hydraulic jack [Item 2 in Fig. 2(b)]. To prevent out-of-plane failure, the frame was restrained by a steel assembly [Item 3 in Fig. 2(b)] installed beneath the hydraulic jack [Item 2 in Fig. 2(b)]. A load cell [Item 1 in Fig. 2(b)] above the hydraulic jack was employed to measure

the applied load. Meanwhile, a load cell [Item 7 in Fig. 2(b)] was installed below each pin support to measure the vertical reactions. To record horizontal reactions at the side column, tension/compression load cell [Item 4 in Fig. 2(b)] was installed in each horizontal roller. A series of linear variable displacement transducers (LVDTs) [Item 5 in Fig. 2(b)] were installed along the beam to measure its deformation shape. Four LVDTs [Item 6 in Fig. 2(b)] were also installed along the side columns to determine the stiffness of horizontal constraints. Moreover, strain gauges were attached along reinforcements before casting.

TEST RESULTS

In this study, a series of half-scaled beam-column sub-assemblages were tested to investigate the load resisting mechanisms of emulative PC frames against progressive collapse. Critical results are tabulated in Table 3 whereas detailed results are discussed in below.

Load Resistance and Failure Mode

RC

Fig. 3 gives the vertical load-displacement curve of test frames. For RC, the yield of beam rebar was first observed at bottom beam rebar close to the middle column. The yield load (YL), which was defined as the load when the beam longitudinal reinforcement yielding was first measured, was 37 kN corresponding to a middle joint displacement (MJD) of 36 mm. When the MJD reached 90 mm, the first peak load (FPL) of 52 kN was measured. The FPL was also called as CAA capacity because the FPL was attributed into the enhanced flexural capacity due to mobilization of CAA. Subsequently, the load resistance of the frame began to drop due to concrete crushing. When the MJD exceeded 280 mm, the vertical load began to re-ascend because of commencement of TCA. Penetrated cracks were observed when the MJD beyond this loading stage. The penetrated cracks were uniformly distributed along the beam length with further

increasing MJD, which indicated tensile axial force developed in the beam. When the MJD reached 410 mm, one of bottom rebars at beam-middle column interface fractured, causing sudden drop of load resistance. The failure of the frame with complete loss of its load resistance occurred at a MJD of 712 mm. The ultimate load (UL, which was defined as the maximum resistance of the frame) or TCA capacity of this frame was 94 kN. The failure mode of RC is shown in Fig. 4. All longitudinal reinforcement at one beam end nearby the middle column was fractured and severe concrete crushing and spalling were observed there.

IA

PC frame IA had similar dimensions and rebar ratio as RC. However, the anchorage length of the bottom rebar in IA was only 230 mm, which was less than the requirement of ACI 318-14 (2014). The YL and FPL of IA were 38 kN and 42 kN, respectively. The FPL of IA was only 81% of that of RC, because the bottom reinforcements were pulled out from middle column, which prevented further strain hardening. However, the pull-out of bottom reinforcements did not prevent the mobilization of TCA and thus, the UL of IA was 98 kN, which was about 104% of that of RC. This could be explained as the pull-out of bottom reinforcements close to the middle column prevents the fracture of these reinforcements but the residual bond between concrete and reinforcements allowed further development of tensile force in these bottom reinforcements at TCA stage. Therefore, it was expected that the UL of IA could have been further increased if the hydraulic jack had greater stroke capacity. However, the measured UL was still used for comparison purpose herein. The failure mode of IA is shown in Fig. 5. It could be found that the beam bottom reinforcements anchored into the middle column were pulled out and no rebar was fractured. Moreover, different to RC, obvious horizontal cracks were formed at the interfaces between PC units and cast-in-situ topping layer.

SA

For SA, the beam bottom reinforcements were bent up to 90° and anchored into the joints. The YL and FPL of SA were 38 kN and 51 kN, respectively, which were very close to that of RC. When the MJD reached 390 mm and 446 mm, beam bottom reinforcements near the middle column fractured in sequence. At a MJD of 660 mm, the UL of 81 kN was measured. Subsequently, top reinforcements of left beam near to the middle column fractured, as a result, SA lost its load resistance suddenly. The UL of SA was approximately 86% of that of RC. This may due to the higher bond stress caused by higher concrete strength in cast-in-situ topping layer casted on site, which led to earlier fracture of the beam top longitudinal reinforcements. The failure mode of SA is shown in Fig. 6. It was found that both top and bottom longitudinal reinforcements near the middle column fractured completely. Moreover, horizontal cracks were also observed between PC units and cast-in-situ topping layer.

UB

UB had U-shaped bars trough with length of 370 mm at the beam ends. Beam bottom reinforcements were bent up 90º and did not pass through or be anchored into the column. Additional U-shaped bars passed through the middle column to assemble the PC beams and columns. The first yield of the beam reinforcements was noticed in the additional U-shaped bars near the beam-middle column interfaces. The YL and FPL of UB were 38 kN and 48 kN, respectively. Rebar fracture first occurred at the U-shaped bar near to the middle column at a MJD of 341 mm. The UL of 75 kN, which was only 80% of that of RC, was measured at a MJD of 651 mm, which was only 91% of that of RC. As mentioned above, the lower UL could be explained as the higher concrete strength in topping layer resulted in higher bond stress and earlier fracture of beam top longitudinal reinforcements. The failure mode of UB is shown in Fig. 7, similar to

aforementioned PC frames, horizontal cracks and concrete crushing were observed at beam ends. Moreover, it was found that plastic hinge was formed at the edge of the trough.

Horizontal Reaction Force

Fig. 8 shows horizontal reaction force-displacement curve of test frames. Negative and positive values represented compressive and tensile reaction force, respectively. As shown in the figure, compressive reaction force was measured first and indirectly demonstrated the mobilization of CAA. The maximum horizontal compressive forces (MHCF) were -178 kN, -158 kN, -176 kN, and -169 kN for RC, IA, SA, and UB, respectively. Therefore, compared to RC frame, PC frame with insufficient anchorage developed less CAA capacity. However, PC frame with sufficient anchorage or additional U-shaped bar in connection zone could develop similar CAA capacity as RC frame. At MJD of 354 mm, 303 mm, 308 mm, and 300 mm, compressive reaction force transferred to tensile. The maximum horizontal tensile forces (MHTF) of RC, IA, SA, and UB were 154 kN, 172 kN, 162 kN, and 138 kN, respectively. Therefore, PC frame with insufficient anchorage could even develop greater TCA capacity than the RC counterpart, which agreed with the vertical load-displacement behavior well.

Deflection of the Double-Span Beam

Fig. 9 shows the beam deflection of UB in various stages. The beam of UB was deformed in a double-curvature manner from the beginning of the test. The beam shown symmetrical profile until the first rebar fracture at a displacement of 341 mm. After that, asymmetry deflection of the beam became evident. After beam bottom rebar close to the middle column fractured, the rotation of the beam concentrated there. It could be found that the measured rotation of the beam ends near the middle column was similar to the chord rotation, which was defined as the ratio of MJD to the clear beam span in DoD (2010). However, the rotation of the beam ends near to the side column

was less than the chord rotation.

Strain Gauge Reading

Fig. 10 shows the strain profile of the beam longitudinal rebar in SA. As shown in the figure, the beam bottom rebar near the middle column yielded first, whereas the beam top rebar near the side column yielded subsequently. This was because the flexural capacity of the joints in the middle column was lower than that of side column, while they experienced similar bending moment demands. At compressive zones, all compressive rebar strains declined when the CAA became exhausted and then tensile strains were observed for all measurement points due to development of the TCA. Similar observations were measured in RC. Fig. 11 gives the rebar strain variation measured in IA. Similar to SA, the rebar near the side column yielded latter than the one near the middle column. Moreover, the strain in B12 dropped suddenly at a MJD of 122 mm, indicating pulling-out failure of the beam bottom rebar. However, tensile strain of about 1200 με was observed after the rebar pulling-out in the subsequent loading history. This could be attributed to the residual bond between the pulling-out rebar and concrete. Fig. 12 shows the strain variation in beam longitudinal rebar and U-shaped rebar of UB. It could be found that the first yield of the rebar occurred in the U-shaped rebar near the middle column since the beam bottom longitudinal rebars were bent up 90° and terminated at the beam ends. In general, the development of strain of the beam top rebar was similar to SA.

DISCUSSION OF TEST RESULTS

Effects of Reinforcing Details

As shown in Fig. 3 and Table 3, the FPL of RC, IA, SA, and UB were 52 kN, 42 kN, 51 kN, and 48 kN, respectively. Therefore, the CAA capacity of IA achieved only 81% of that of RC because beam bottom reinforcements near to the middle column were pulled out. However, the

CAA capacity of SA and UB was approximately 98% and 92% of RC and thus, PC frame with sufficient anchorage or additional U-shaped bar connection could develop similar CAA capacity as RC frame. The UL of RC, IA, SA, and UB were 94 kN, 98 kN, 81 kN, and 75 kN, respectively. It was found that IA could attain the highest UL although pulling-out failure occurred at the beam end near to the middle column. This was because the pull-out of bottom reinforcements prevented the fracture of these rebar, while the residual bond between these pulling-out rebar and concrete could still increase the horizontal tensile reaction force at TCA stage. As mentioned previously, the relatively lower UL of SA and UB was mainly due to the higher bond stress between beam top rebar and cast-in-situ topping layer, which led to the earlier rebar fracture and lower deformation capacity.

Load Resistance De-Composition

As shown in Fig. 13, force analysis was carried out to de-composite the contribution of load resistance. It can be seen that the load resistance *P* equals to the summation of vertical projections of the shear force (*V*) and axial force (*N*) at the critical sections.

$$P = (N\sin\theta + V\cos\theta) \quad (1)$$

where θ is the local rotation of the beam segment near to the middle column and it can be determined by the measured displacements of D_3 and D_4 ($\theta = \arctan\left(\frac{4(D_4 - D_3)}{L}\right)$); D_3 is the vertical displacement at the position with $L/4$ away from the middle column whereas D_4 is the MJD; L is beam clear span.

The shear force (*V*) and axial force (*N*) can be determined by Eqs. 2 and 3:

$$N = (V_L \tan\theta + H_t + H_b)\cos\theta \quad (2)$$

$$V = (V_L - N\sin\theta) / \cos\theta \quad (3)$$

The bending moment at the beam end near to the middle column (M_M) and the one near to the side column (M_S) can be determined by Eqs. 4 and 5:

$$M_M = V_L l - H_t(D_4 + 0.35) - H_b(D_4 - 0.35) \quad (4)$$

$$M_S = 0.2V_L - 0.3H_t + 0.1H_b \quad (5)$$

where H_t and H_b are the horizontal reaction forces at the top and bottom roller, respectively; V_L is the vertical reaction force measured at the pin support; l is distance from the center of the left side column to the critical section.

The de-composition of the load resistance of IA, SA, and UB are given in Fig. 14. It can be seen that, at small deformation stage, the shear force provided majority of the load resistance. With the increase of MJD, the contribution of shear force decreased because of evanishment of the flexural action due to concrete crushing, while the load resistance from the axial force transferred from negative to positive because the beginning of TCA. At large deformation stage, the tensile axial force dominated the load resistance and the contribution from shear force kept decreasing. However, based on this analysis, it was incorrect to conclude that at large deformation stage, the load resistance purely attributed into TCA.

The variation of bending moments at the beam ends are shown in Fig. 15. The overall trend of the bending moment was similar to that of load resistance from the shear force. As mentioned above, the contribution of the shear force actually reflected the load resisting contribution of flexural action. As shown in Fig. 15, due to pulling-out failure of the beam bottom reinforcements, the maximum bending moment of IA at the beam end near to the middle column was much lower than that of SA and UB.

Tie Force

The ultimate chord rotation which was defined as the ultimate displacement to the beam clear span of RC, IA, SA, and UB were 0.24, 0.23, 0.24, and 0.22, respectively. As tested results had indicated that 0.20 radian rotational capacity requirement of DoD (2010) could be satisfied for tested RC and PC frames, the tie-force requirements of DoD (2010) were evaluated herein. The required tie-force can be determined by Eq. 6.

$$Fp = 6W_F L_1 L_p \tag{6}$$

where W_F is the floor load (7.6 kN/m^2 as a result of load combination of $(1.2DL + 0.5LL)$); L_1 is the distance between column centers; L_p is the allowed floor width (0.91 m in DoD (2010) and 0.46 m herein as 1/2 scaled frames).

The required tie forces were listed in Table 3. It was found that the measured tie-forces (UL herein) were greater than the required tie-forces for all frames. Therefore, PC beams with emulative connections could provide sufficient tie-force to resist progressive collapse.

Proposal New TCA Model and Evaluation of Existing CAA Models for PC Frames

To facilitate practical applications of TCA, a simplified model was proposed herein to predict the TCA capacity. Based on the test results, it was found that the UL was mainly controlled by the top reinforcements as the bottom reinforcements fracture earlier and therefore, only tensile forces in the top reinforcements were considered in the proposed model. As illustrated in Fig. 16, the angle θ of the tensile forces can be determined by the points of resultant forces in the beam end sections. Thus, the proposed model can be expressed as follows

$$P_{TCA} = 2 f_u A_{st} \sin\theta \tag{7}$$

where f_u and A_{st} are the ultimate strength and area of the top reinforcement at the section near to the middle column, respectively.

The calculated results from the proposed model were compared with the test results in Fig. 3. The calculated results agreed with the test results well although slightly under-estimation was obtained. Actually, for safety's sake, conservative result is preferred for design.

Compared to TCA, CAA raises much lower demand in continuity of rebar and deformation capacity. Therefore, it is preferred to prevent progressive collapse relying on CAA. Yu and Tan (2014) and Lu et al. (2018) proposed analytical models to assess the CAA capacity. For the models, please refer to corresponding paper due to spacing limitation. The reliability of these models for evaluation of CAA capacity of PC frames was quantified herein. As shown in Fig. 17a, both models may overestimate the CAA capacity of IA due to pulling-out failure of the bottom reinforcements near to the middle column. As shown in Figs. 17(b-d), both analytical models predicted the CAA capacity of remaining specimens reasonably. However, as Yu and Tan (2014)'s model relied on iteration, for simplicity, Lu et al. (2018)'s model was recommended for PC specimens with emulative connections.

CONCLUSIONS

Based on test results and analytical analysis, the following conclusions can be drawn:

1. In general, the load resisting mechanisms of emulative PC frames with emulative connections were similar to that of RC frame. Beam action, compressive arch action, and tensile catenary action were mobilized in sequence for PC frames to resist progressive collapse.
2. For IA, pulling-out failure prone to occur at the bottom reinforcements near to the middle joint, which prevented the sufficient development of CAA capacity. However, the pulling-out of bottom reinforcements could provide additional TCA capacity, which was beneficial for

ultimate load capacity at large deformation stage.

3. UB and SA could develop comparable yield load and CAA capacity as that of RC. Comparing to RC frame, PC frames with emulative joints may achieve relatively lower deformation capacity due to higher concrete strength used for cast-in-situ topping layer.
4. PC frames with emulative connections had comparable rotation capacity as RC frame and PC beams could provide sufficient tie-force as required by DoD (2010).
5. The proposed TCA model was able to predict the TCA capacity reasonably. Both CAA models from Lu et al. (2018) and Yu and Tan (2014) could predict CAA capacity well. However, considering the convenience, Lu et al. (2018)'s model was recommended.

Data Availability

Some or all data, models, or code that support the findings of this study are available from the corresponding author upon reasonable request.

ACKNOWLEDGMENTS

This research was supported by a research grant provided by the Natural Science Foundation of China (Nos. 51778153,52022024). Any opinions, findings and conclusions expressed in this paper are those of the writers and do not necessarily reflect the view of Natural Science Foundation of China.

REFERENCES

ACI (American Concrete Institute). 2014. "Building code requirements for structural concrete (ACI 318-14) and commentary (318R-14)." ACI Committee 318. Farmington Hills, MI: ACI.

ASCE. 2010. "Minimum design loads for buildings and other structures." ASCE/SEI 7. Reston, VA: ASCE.

343 DoD (Department of Defense). 2010. “Design of building to resist progressive collapse.” UFC 4-
344 023-03. Washington, DC: DoD.
345 GSA (US General Service Administration) 2013. “Progressive collapse analysis and design
346 guidelines for new federal office buildings and major modernization projects.” Washington,
347 DC: GSA.
348 Deng, X.F., Liang, S.L., Fu, F. and Qian, K. 2020. “Effects of high-strength concrete on
349 progressive collapse resistance of reinforced concrete frame.” Journal of Structural
350 Engineering, 146(6):4020078
351 Fu, F. 2016. “Structural analysis and design to prevent disproportionate collapse.” CRC Press.
352 ISBN 978-1-4987-8820-5.
353 Kang, S. B., and K. H. Tan. 2015. “Behaviour of precast concrete beam–column sub-assemblages
354 subject to column removal.” Eng. Struct. 93 (Mar): 85-96.
355 Kang, S. B., and K. H. Tan. 2017. “Progressive collapse resistance of precast concrete frames with
356 discontinuous rebar in the joint.” J. Struct. Eng. 143 (9): 04017090.
357 Lew, H. S., J. A. Main, Y. H. Bao, F. Sadek, V. P. Chiarito, S. D. Robert, and J. O. Torres. 2017.
358 “Performance of precast concrete moment frames subjected to column removal: Part 1,
359 experimental study.” PCI J. 62 (5): 35-52.
360 Lin, K. Q., Lu, X. Z., Li, Y., Zhou, W. D., and Guan, H. 2019. “A novel structural detailing for the
361 improvement of seismic and progressive collapse performance of RC frames.” Earthquake
362 Eng. Struct. Dyn. 48 (13): 1451-1470.
363 Lu, X. Z., K. Q. Lin, C. F. Li, and Y. Li. 2018. “New analytical calculation models for compressive
364 arch action in reinforced concrete structures.” Eng. Struct. 168 (Aug): 721-735.
365 Lu, X. Z., K. Q. Lin, Y. Li, H. Guan, P. Q. Ren, and Y. L. Zhou. 2017. “Experimental investigation

366 of RC beam-slab substructures against progressive collapse subjected to an edge-column-
367 removal scenario." Eng. Struct. 149 (Aug): 91-103.
368 Orton, S., J. O. Jirsa, and O. Bayrak. 2009. "Carbon fiber-reinforced polymer for continuing in
369 existing reinforced concrete buildings vulnerable to collapse." ACI Struct. J. 106 (5): 608–616.
370 PCI (Precast Prestressed Concrete Institute). PCI design handbook. 7th ed.; 2010.
371 Qian, K., and B. Li. 2018. "Performance of precast concrete substructures with dry connections to
372 resist progressive collapse." J. Perform. Constr. Facil. 32 (2): 4018005.
373 Qian, K., and B. Li. 2019. "Investigation into resilience of precast concrete floors against
374 progressive collapse." ACI Struct. J. 116 (2): 171-182.
375 Qian, K., Liang, S.L, Fu, F. and Fang, Q. 2019. "Progressive collapse resistance of precast concrete
376 beam-column sub-assemblages with high-performance dry connections." Engineering
377 Structures, 198: 109552
378 Qian, K., and B. Li. 2012a. "Dynamic performance of RC beam-column substructures under the
379 scenario of the loss of a corner column—Experimental results." Eng. Struct. 42 (May): 154-
380 167.
381 Qian, K., and B. Li. 2012b. "Slab effects on response of reinforced concrete substructures after
382 loss of corner column." ACI Struct. J. 109 (6): 845-855.
383 Qian, K., and B. Li. 2013. "Performance of three-dimensional reinforced concrete beam-column
384 substructures under loss of a corner column scenario." J. Struct. Eng. 139 (4): 584-594.
385 Qian, K., and B. Li. 2015. "Quantification of slab influence on the dynamic performance of RC
386 frames against progressive collapse." J. Perform. Constr. Facil. 29 (1): 04014029.
387 Qian, K., B. Li, and J. X. Ma. 2015. "Load-carrying mechanism to resist progressive collapse of
388 RC buildings." J. Struct. Eng. 141 (2): 04014107.

389 Qian, K., B. Li, and Z. Zhang. 2016. “Influence of multicolumn removal on the behavior of RC
390 floors.” J. Struct. Eng. 142 (5): 04016006.
391 Qian, K., S. L. Liang, X. Y. Xiong, F. Fu, and Q. Fang. 2020. “Quasi-static and dynamic behavior
392 of precast concrete frames with high performance dry connections subjected to loss of a
393 penultimate column scenario.” Eng. Struct. 205 (Dec): 110115.
394 Weng, Y. H., K. Qian, F. Fu, and Q. Fang. 2020. “Numerical investigation on load redistribution
395 capacity of flat slab substructures to resist progressive collapse.” Journal of Building
396 Engineering, 29: 101109.
397 Ren, P. Q., Y. Li, X. Z. Lu, H. Guan, and Y. L. Zhou. 2016. “Experimental investigation of
398 progressive collapse resistance of one-way reinforced concrete beam-slab substructures under
399 a middle-column-removal scenario.” Eng. Struct. 118 (Apr): 28–40.
400 Sadek, F., J. A. Main, H. S. Lew, Y. H. Bao. 2011. “Testing and analysis of steel and concrete
401 beam-column assemblies under a column removal scenario.” J. Struct. Eng. 137 (9): 881-892.
402 Sasani M, and S. Sagiroglu. 2008. “Progressive collapse resistance of Hotel San Diego.” J. Struct.
403 Eng. 134 (3): 478-488.
404 Sasani M. 2008. “Response of a reinforced concrete infilled-frame structure to removal of two
405 adjacent columns.” Eng. Struct. 30 (Mar): 2478–2491.
406 Shan, S. D., S. Li, S. Y. Xu, and L. L. Xie. 2016. “Experimental study on the progressive collapse
407 performance of RC frames with infill walls.” Eng. Struct. 111 (Jan): 80-92.
408 Stevens, D., B. Crowder, D. Sunshine, K. Marchand, R. Smilowitz, E. Williamson, and M.
409 Waggoner. 2011. “DoD research and criteria for the design of buildings to resist progressive
410 collapse.” J. Struct. Eng. 137 (9): 870-880.
411 Su, Y. P., Y. Tian, and X. S. Song. 2009. “Progressive collapse resistance of axially-restrained

412 frame beams.” ACI Struct. J. 106 (5): 600-607.
413 Valipour, H., N. Vessali, S. J. Foster, and B. Samali. 2015. “Influence of concrete compressive
414 strength on the arching behaviour of reinforced concrete beam assemblages.” Advances in
415 Structural Engineering, 18 (8): 1199-1214.
416 Yu, J., and K. H. Tan. 2013. “Structural behavior of RC beam-column sub-assemblages under a
417 middle column removal scenario.” J. Struct. Eng. 139 (2): 233–250.
418 Yu, J., and K. H. Tan. 2014. “Analytical model for the capacity of compressive arch action of
419 reinforced concrete sub-assemblages.” Magazine of Concrete Research, 66 (3): 109–126.
420 Yu, J., and K. H. Tan. 2017. “Structural behavior of reinforced concrete frames subjected to
421 progressive collapse.” ACI Struct. J. 114 (1): 63–74.
422 Yu, J., Luo, L. Z., and Fang, Q. 2020. “Structural behavior of reinforced concrete beam-slab
423 assemblies subjected to perimeter middle column removal scenario.” Eng. Struct. 208: 110336.
424 Yu, J., T. Rinder, A. Stolz, K. H. Tan, and W. Riedel. 2014. “Dynamic progressive collapse of an
425 RC assemblage induced by contact detonation.” J. Struct. Eng. 140 (6): 04014014.
426
427
428
429
430
431
432
433
434

Table 1. Frame Details

Test ID	Reinforcing details in middle joint	Beam clear span (mm)	Span/depth ratio	Beam longitudinal rebar			
				A-A section		B-B section	
				Top	Bottom	Top	Bottom
RC	Continuity	2750	11	3T12	2T12	2T12	2T12
IA	Insufficient anchorage	2750	11	3T12	2T12	2T12	2T12
SA	Sufficient anchorage	2750	11	3T12	2T12	2T12	2T12
UB	U-shaped bar	2750	11	3T12	4T12	2T12	2T12

Table 2. Material Properties of Rebar

Items		Nominal diameter (mm)	Yield strength (MPa)	Ultimate strength (MPa)	Elongation (%)
Transverse rebar	R6	6	346	485	18.4
Longitudinal	T12	12	438	576	15.3
reinforcements	T16	16	466	603	16.8

Note: R6 represents plain rebar with diameter of 6 mm; T12 and T16 represent deformed rebar with diameter of 12 mm and 16 mm, respectively.

Table 3. Test Results

Test ID	MJD at FPL (mm)	MJD at UL (mm)	Resistance re-ascending (mm)	FPL (kN)	UL (kN)	MHCF (kN)	MHTF (kN)	F_P (kN)
RC	90	712	280	52	94	-178	154	63
IA	68	690	266	42	98	-158	172	63
SA	66	660	220	51	81	-176	162	63
UB	76	651	244	48	75	-169	138	63

Note: MJD represents vertical displacement; FPL and UL represent first peak load and ultimate load, respectively; MHTF and MHCF represent maximum horizontal tensile force and maximum horizontal compressive force, respectively. F_P is the required peripheral tie force.

Figure 1

Click here to access/download;Figure;JSE-Fig.1.pdf

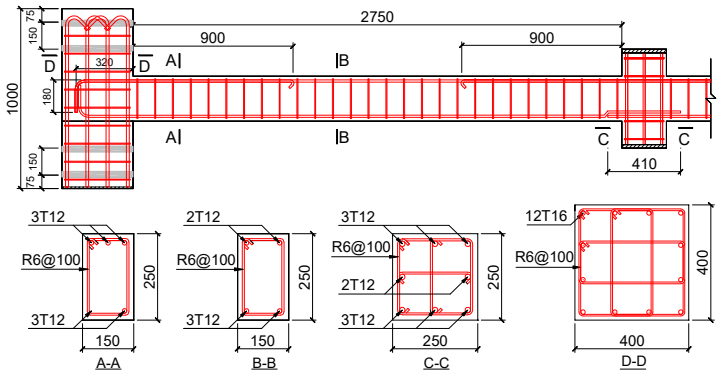

(a)

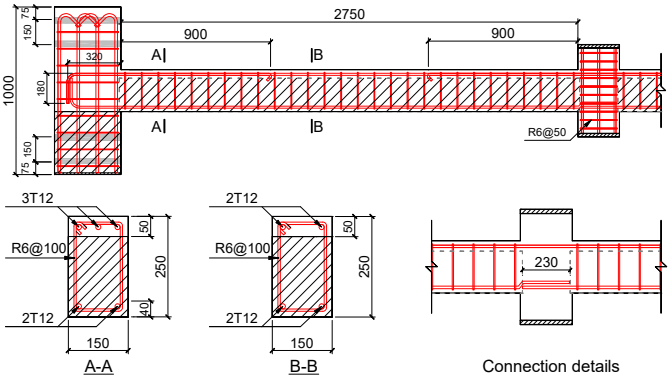

(b)

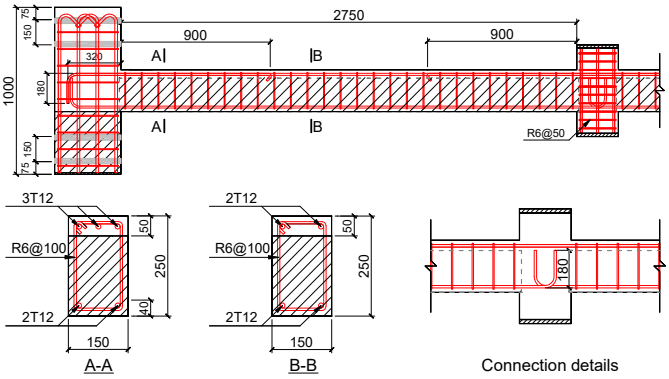

(c)

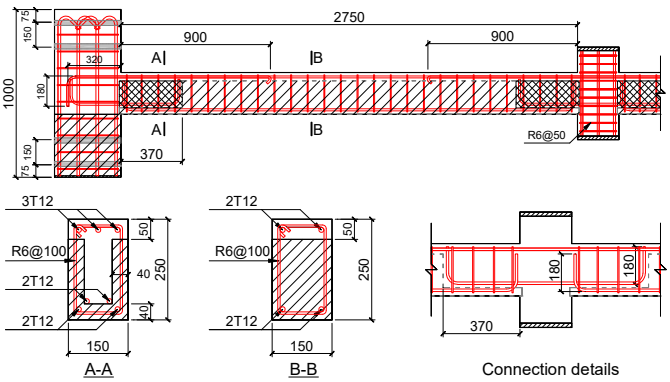

(d)

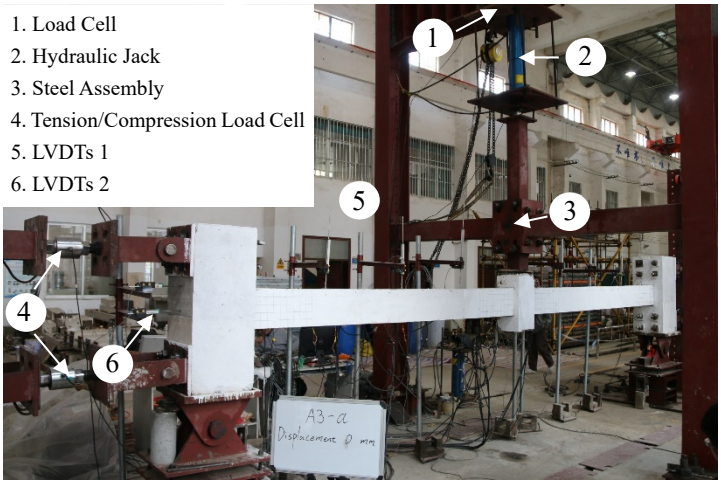

(a)

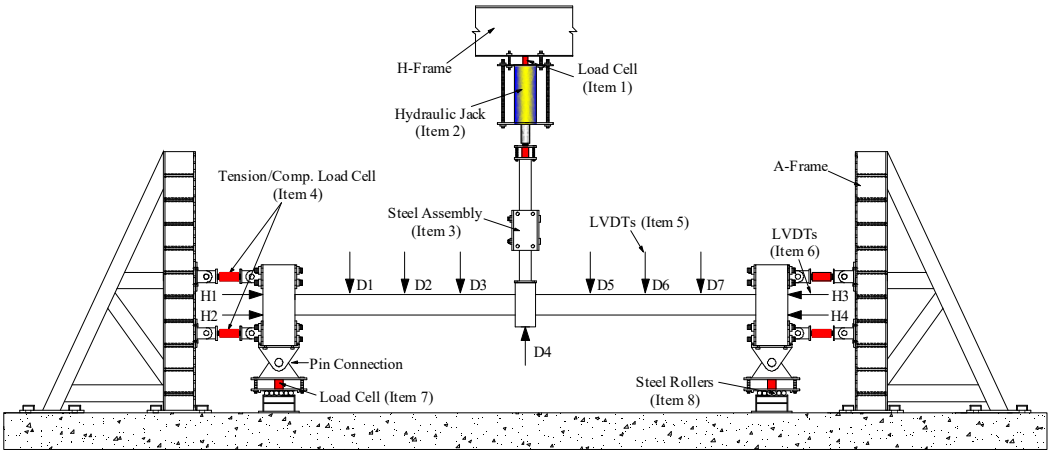

(b)

Figure 3

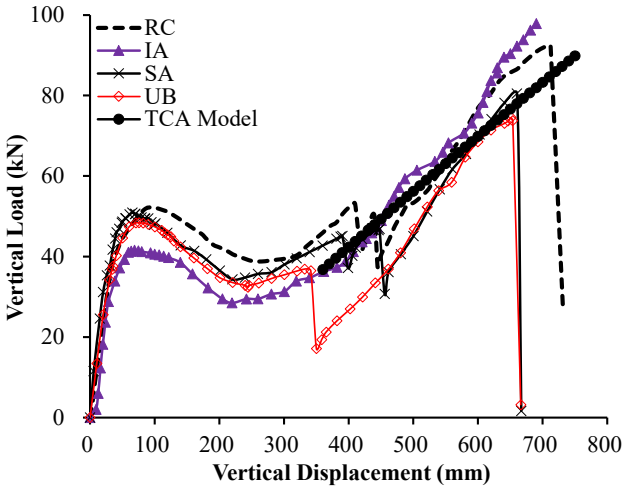

Figure 4

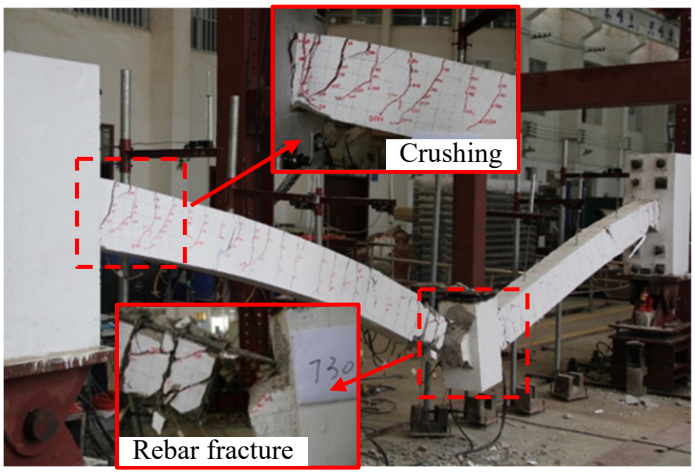

Figure 5

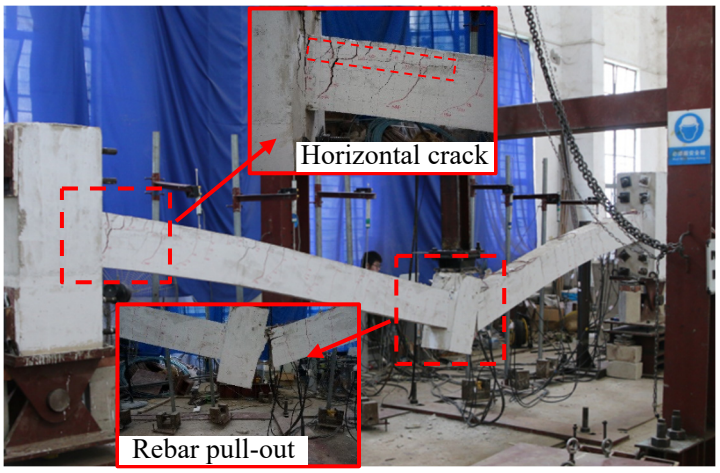

Figure 6

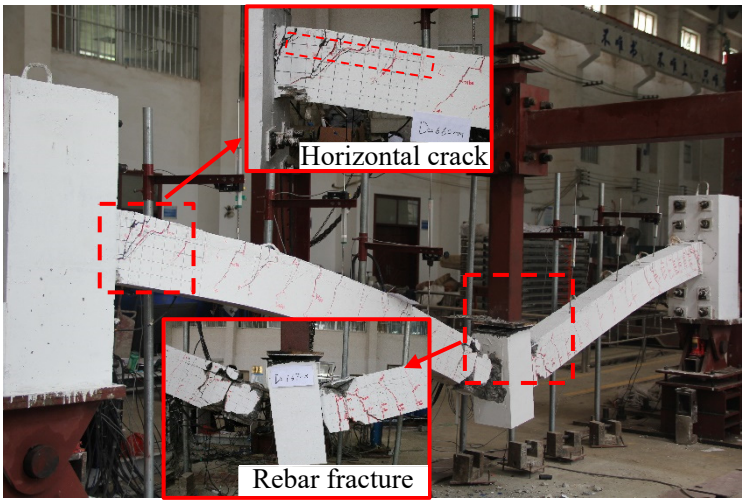

Figure 7

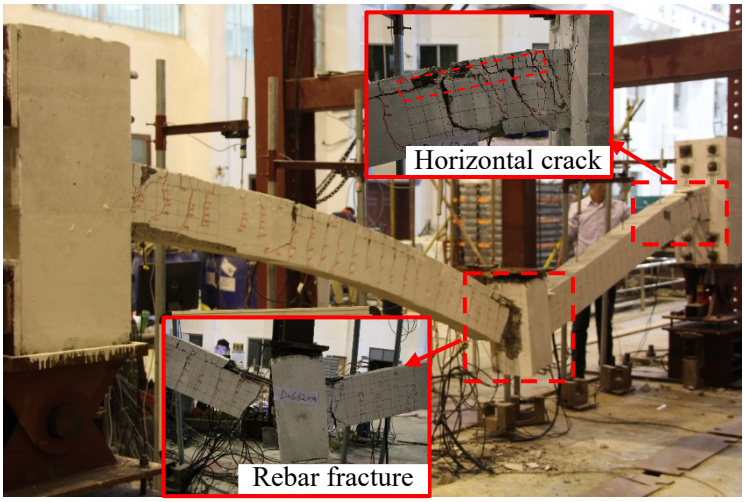

Figure 8

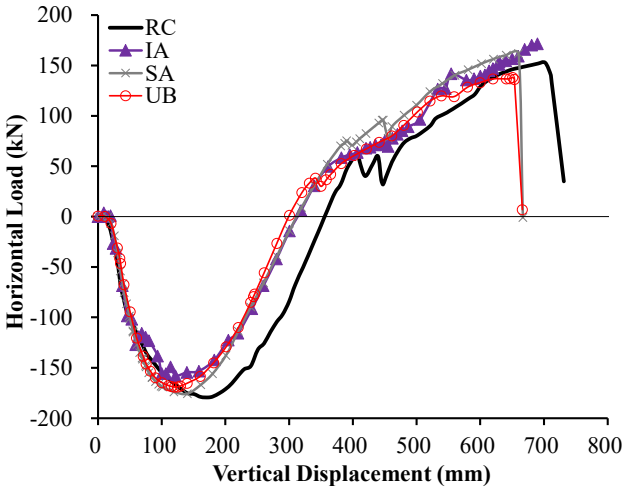

Figure 9

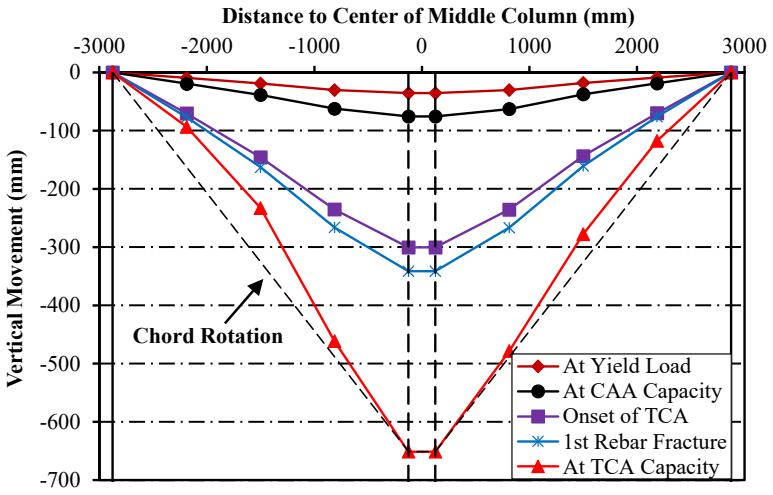

Figure 10

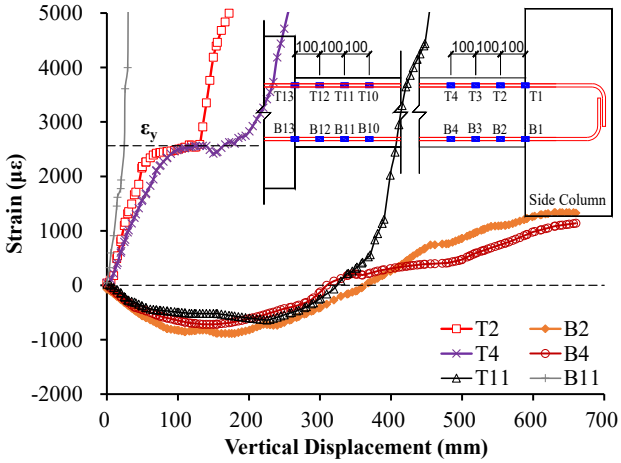

Figure 11

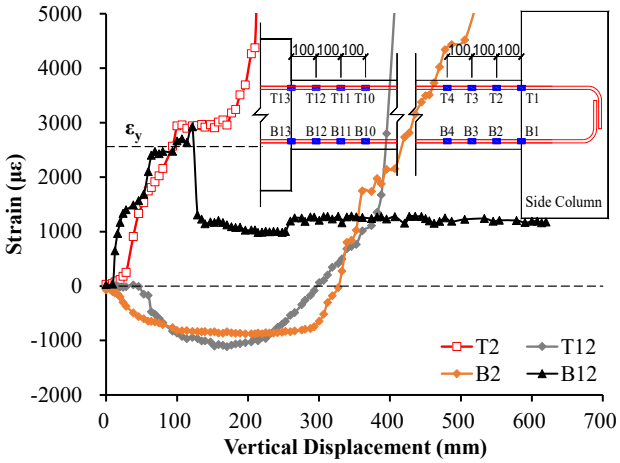

Figure 12

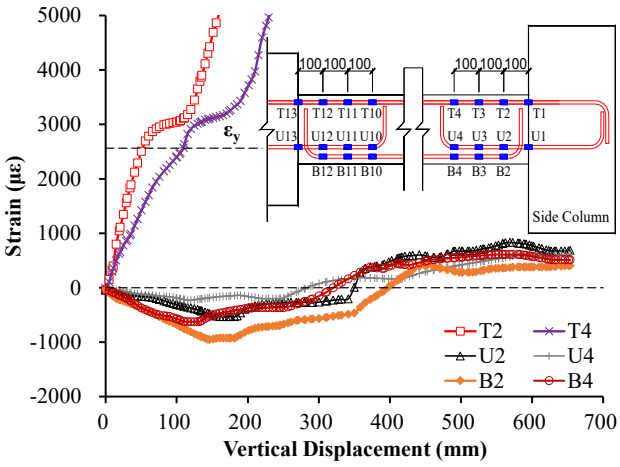

(a)

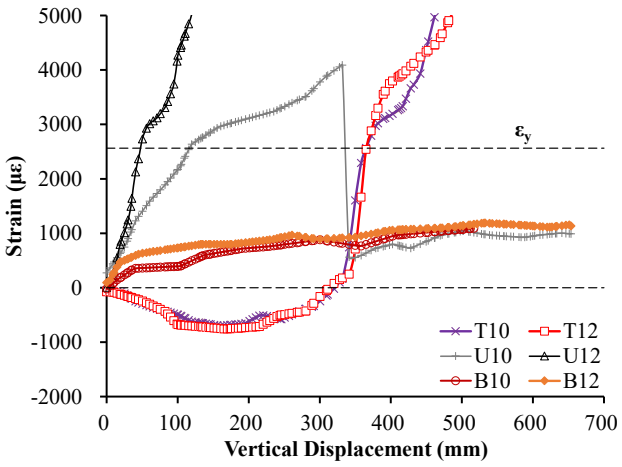

(b)

Figure 13

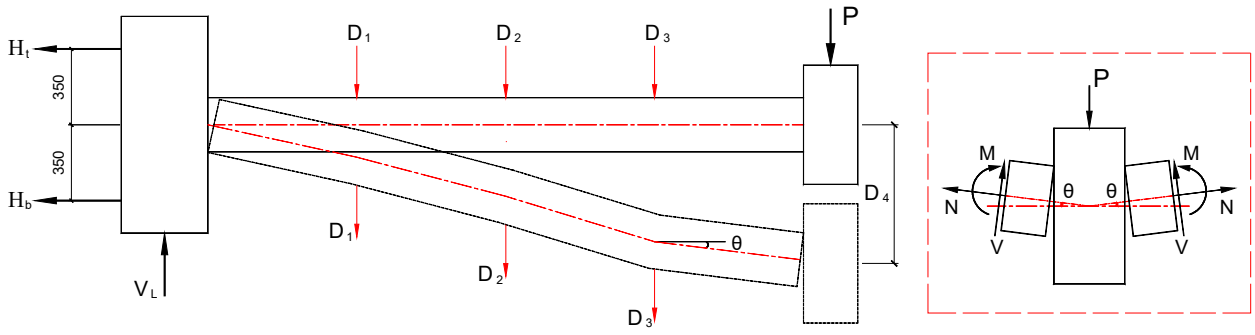

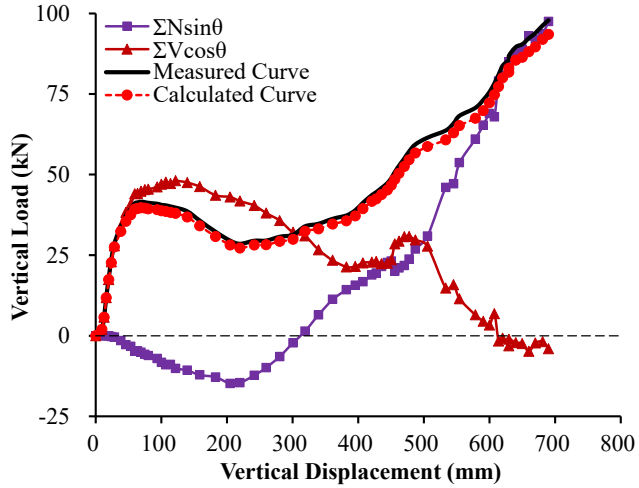

(a)

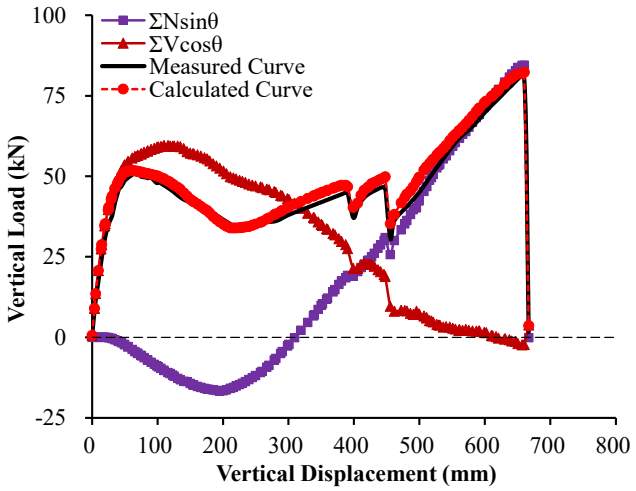

(b)

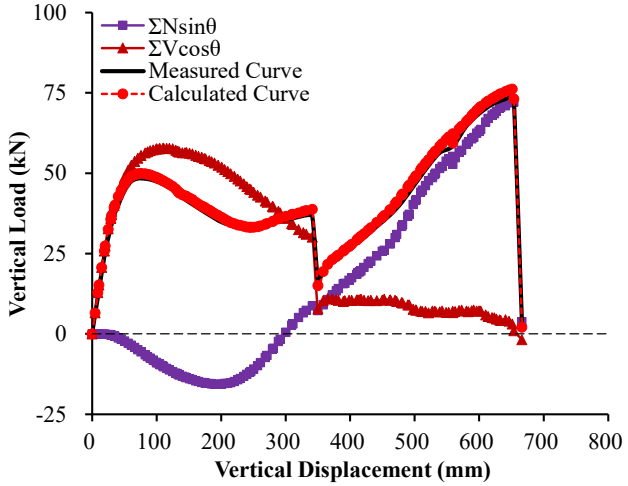

(c)

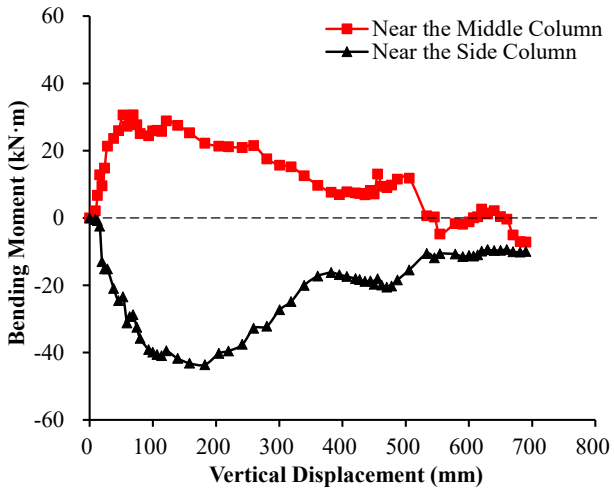

(a)

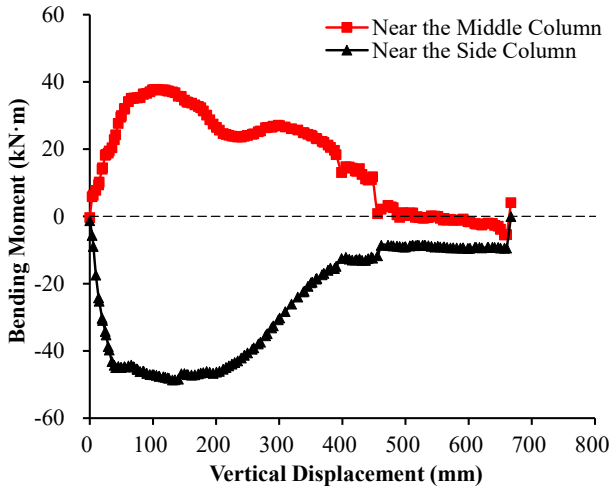

(b)

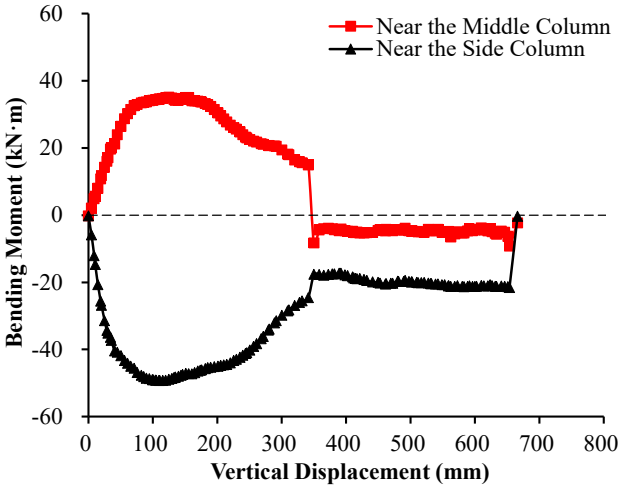

(c)

Figure 16 Click here to access/download;Figure;JSE-Fig.16.pdf

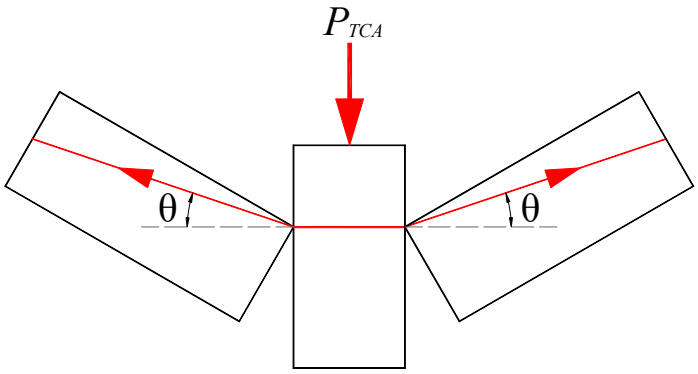

Figure 17

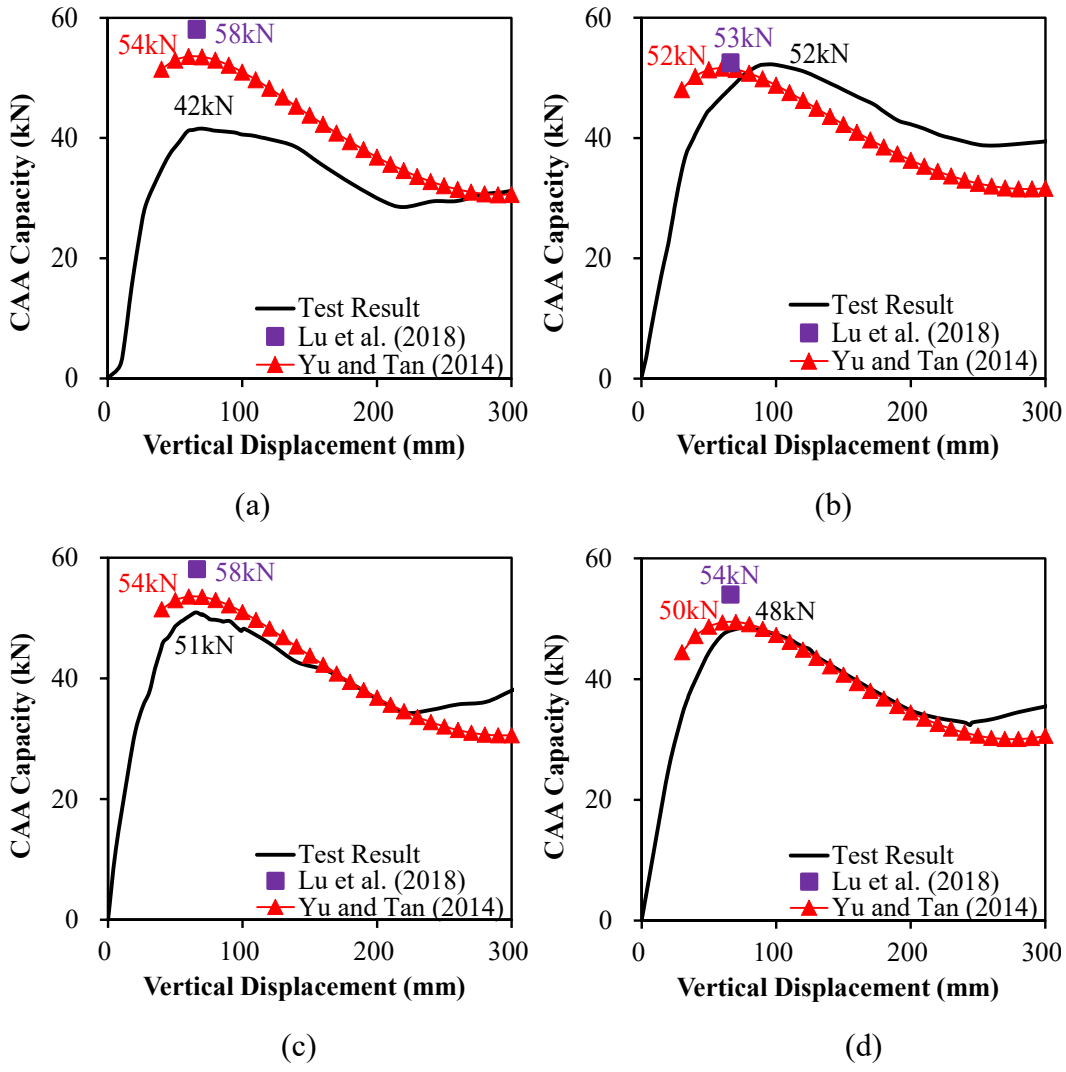

Figure Captions

Fig. 1. Details of test frame: (a) RC; (b) IA; (c) SA; (d) UB

Fig. 2. Test setup: (a) photo, (b) drawing

Fig. 3. Vertical load-displacement curves

Fig. 4. Failure mode of RC

Fig. 5. Failure mode of IA

Fig. 6. Failure mode of SA

Fig. 7. Failure mode of UB

Fig. 8. Horizontal reaction force-displacement curves

Fig. 9. Deformation shape of double-span beam of UB

Fig. 10. Strain of beam rebar in SA

Fig. 11. Strain of beam rebar in IA

Fig. 12. Strain of beam rebar in UB: (a) near the side column; (b) near the middle column

Fig. 13. Relationship between internal forces at critical section and load resistance

Fig. 14. Load resistance de-composition: (a) IA; (b) SA; (c) UB

Fig. 15. Bending moment at the beam ends: (a) IA; (b) SA; (c) UB

Fig. 16. Proposed TCA model

Fig. 17. Comparison of measured CAA capacity with theoretical one: (a) IA; (b) RC; (c) SA; (d) UB